Bio-electronics

Deutsche Ausgabe: DOI: 10.1002/ange.201604833
Internationale Ausgabe: DOI: 10.1002/anie.201604833

# The Strong Influence of Structure Polymorphism on the Conductivity of Peptide Fibrils

*Denis Ivnitski, Moran Amit, Ohad Silberbush, Yoav Atsmon-Raz, Jayanta Nanda, Rivka Cohen-Luria, Yifat Miller, Gonen Ashkenasy,* and Nurit Ashkenasy**

**Abstract:** *Peptide fibril nanostructures have been advocated as components of future biotechnology and nanotechnology devices. However, the ability to exploit the fibril functionality for applications, such as catalysis or electron transfer, depends on the formation of well-defined architectures. Fibrils made of peptides substituted with aromatic groups are described presenting efficient electron delocalization. Peptide self-assembly under various conditions produced polymorphic fibril products presenting distinctly different conductivities. This process is driven by a collective set of hydrogen bonding, electrostatic, and π-stacking interactions, and as a result it can be directed towards formation of a distinct polymorph by using the medium to enhance specific interactions rather than the others. This method facilitates the detailed characterization of different polymorphs, and allows specific conditions to be established that lead to the polymorph with the highest conductivity.*

The de novo design and preparation of β-sheet peptide and protein fibril structures, and their use as functional materials, constitute a topic of ongoing importance for both basic and applied science.[1] Detailed analysis of the fibrillation process, controlled by both intrinsic parameters (that is, the protein sequence) and environmental conditions, was originally directed at understanding protein misfolding in neurodegenerative diseases.[2] In a related research direction, scientists have highlighted the probable involvement of amphiphilic peptides in early chemical evolution.[3] Studies using prebiotic peptides have thus revealed multiple pathways leading to fibril assembly and often to the emergence of functions. During the past few years, attempts have been made to precisely guide amphiphilic peptide self-assembly into well-defined architectures suitable for various applications in biotechnology and nanotechnology, such as scaffolding cell tissues,[1c,4] drug delivery,[4b,5] catalysis,[6] and bio-electronics.[7] However, studies on peptide sequences of both natural origin (for example, Aβ-amyloid segments) and synthetic compounds often reveal structure polymorphisms among assemblies formed under similar, and sometimes even identical, conditions.[8] For particular applications where control over the bulk properties of the fibril material is sufficient to facilitate the desired function, for example, applications based on macroscopic gel properties, polymorphism is usually not critical. However, in other cases, primarily when peptide fibrils are used for catalysis or electron transfer, even minor changes in topology or the local environment due to polymorphisms can affect the function, either positively or detrimentally. As part of our long-term program aiming at utilizing peptide-aromatic nanostructures as components of next generation electronic devices, we address the challenge of the straightforward elucidation of the following relations: peptide assembly conditions leading to fibril microstructure and morphology and furthermore to assembly-dependent device functionality (conductance). The new approach allows us to characterize different polymorphs and, furthermore, to find specific conditions producing the polymorph(s) with the highest conductivity.

We describe the utility of fibrils prepared from a newly designed amphiphilic peptide ($\mathbf{P^{NDI}}$, Figure 1) equipped with a single polyaromatic naphthalene diimide (NDI) moiety as electron conducting materials. Remarkably, we show that the incorporation of the NDI moiety facilitates efficient electron transport along the structure, resulting in a significant increase ($\geq 2$ orders of magnitude) in the fibril conductivity relative to its analogue lacking NDI (**KFE-8**, Figure 1). We have found that $\mathbf{P^{NDI}}$ self-assembly under various conditions (water and co-solvent mixtures) leads to polymorphic fibril products exhibiting distinctly different conductivities. Using molecular dynamics (MD) simulations and spectroscopy and microscopy studies, we show that the intimate interactions between adjacent NDI moieties differ significantly in assemblies formed under different conditions, affecting both the π stacking level and the chiral arrangement. The different interaction patterns, in turn, affect the fibril morphology, leading to substantial differences in fibril width, as well as twist level and directionality. We augment the self-assembly related data with electrical characterizations to explain the differences in fibril polymorph conductivity.

[*] D. Ivnitski, Dr. Y. Atsmon-Raz, Dr. J. Nanda, Dr. R. Cohen-Luria, Dr. Y. Miller, Prof. G. Ashkenasy
Department of Chemistry, Ben-Gurion University of the Negev
Beer-Sheva 84105 (Israel)
E-mail: gonenash@bgu.ac.il
Dr. M. Amit, O. Silberbush, Prof. N. Ashkenasy
Department of Materials Engineering
Ben-Gurion University of the Negev
Beer-Sheva 84105 (Israel)
E-mail: nurita@bgu.ac.il
Dr. Y. Atsmon-Raz
Department of Biological Science, University of Calgary
Center of Molecular Simulation
2500 University Drive NW, Calgary, Alberta, T2N 1N4 (Canada)
Dr. Y. Miller, Prof. G. Ashkenasy, Prof. N. Ashkenasy
The Ilse Katz Institute for Nanoscale Science and Technology
Ben-Gurion University of the Negev
Beer-Sheva 84105 (Israel)

Supporting information for this article can be found under: http://dx.doi.org/10.1002/anie.201604833.

  

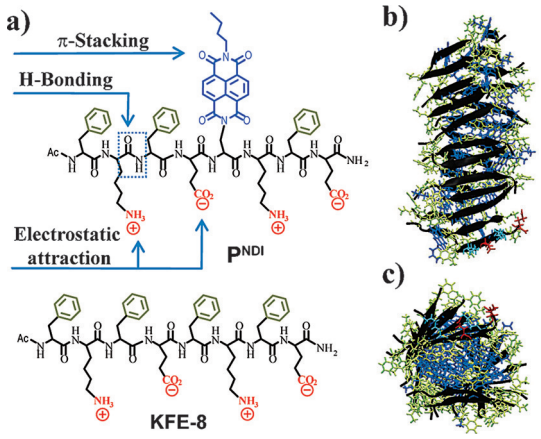


***Figure 1.*** a) Molecular structures of the $\mathbf{P^{NDI}}$ and **KFE-8** peptides. b), c) Side and top views, respectively, of the most stable fibrillar structure of self-assembled $\mathbf{P^{NDI}}$ (black arrows = fibril β-strands; green = Phe residues, blue = NDI moieties; most other residues omitted for clarity). MD simulations were performed in the NPT ensemble at 310 K for 80 ns, using the NAMD program with all-atom CHARMM27 force-field (see the Supporting Information).[11].

A variety of sequence patterns have been previously utilized for constructing peptide-aromatic conjugates that self-assemble into fibril structures.[7a,b,9] The novel $\mathbf{P^{NDI}}$ octapeptide sequence is based on an alternating hydrophobic–hydrophilic pattern with a β-sheet formation tendency (Figure 1). An additional driving force for self-assembly is provided by alternating the negatively (E) and positively (K) charged residues that can interact complementarily. Previous studies have shown rapid self-assembly of the **KFE-8** model compound (and similar peptides) to give helical ribbons or fibers, which were then exploited for structural investigations and biomedical applications.[10] The NDI moiety of $\mathbf{P^{NDI}}$ is attached in place of the F5 phenyl group of **KFE-8** in such a way that (within an anti-parallel β-sheet arrangement) NDI groups from adjacent molecules will optimally overlap and interact through their π systems (Figure 1). $\mathbf{P^{NDI}}$ was readily synthesized on solid phase (Supporting Information, Scheme S1 and Figure S1), cleaved off the resin, and purified by HPLC.

The tendency of $\mathbf{P^{NDI}}$ to form fibrils was first studied using MD simulations at pH 7. Three models were constructed for $\mathbf{P^{NDI}}$ (M1–M3; Supporting Information, Figure S4). The results show that the M1 model, in which the monomers are oriented anti-parallel to each other, both within the same layer and in opposing layers, was energy minimized into a well-defined bilayer fibril structure (Figure 1b). The models minimized with alternative relative monomer orientations formed either slightly less stable (M2; anti-parallel:parallel) or dramatically less stable (M3; parallel:parallel) structures (Supporting Information, Tables S1, S2). The hydrophobic core in the most stable $\mathbf{P^{NDI}}$ fibril structure consisted predominantly of stacked NDI groups (Figure 1c), potentially facilitating efficient electron transfer along the fibrils. As was previously found for **KFE-8**, the simulations revealed a left-handed twisted $\mathbf{P^{NDI}}$ fibril structure (Figure 1b). Nevertheless, as established in our experiments discussed below, this particular fibril characteristic is drastically affected by the self-assembly conditions.

The spontaneous self-assembly of $\mathbf{P^{NDI}}$ in four different aqueous mixtures was investigated using fluorescence and CD spectroscopy (Figure 2). $\mathbf{P^{NDI}}$ was equilibrated for ≥30 min in

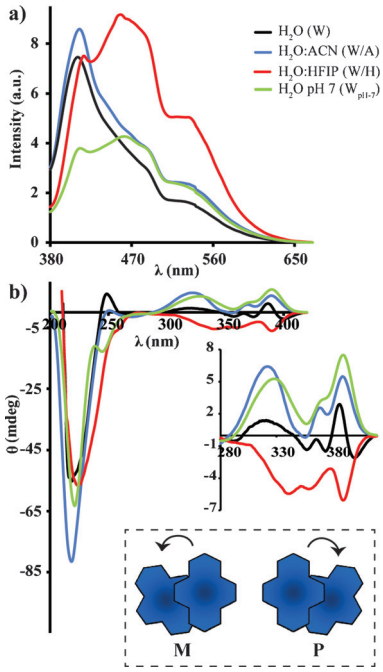


***Figure 2.*** Spectroscopic characterizations of 350 μM $\mathbf{P^{NDI}}$ assembly equilibrated in different solutions. a) Emission spectra ($\lambda_{ex}$ = 350 nm). b) CD spectra. The CD 280–400 nm range is expanded to highlight the Cotton effect peaks corresponding to the polarized transition along the NDI moiety *z* axis. CD spectra of $\mathbf{P^{NDI}}$ in W/A and W/H with different water to co-solvent ratios revealed the same trends with respect to positive and negative Cotton effects in the 280–400 nm range, respectively (Supporting Information, Figure S5). Inset: representation of the relative arrangements of stacked NDI units.

pure water at a pH of about 5.5 (designated as W) or at pH 7.0 ($W_{pH=7}$), or in water mixtures with co-solvents that promote hydrogen bonding (water/acetonitrile 3:2; W/A)[12] or decrease the likelihood of monomers interaction via hydrogen bonds (water/hexafluoro-2-propanol (HFIP) 4:1; W/H).[13] The fluorescence spectra of the self-assembled compounds show three emission peaks (Figure 2a), one at 415 nm that is attributed to monomeric NDI emission, and two others at 485 nm and 530 nm, indicative of excimer formation due to π-stacking interactions.[14] The latter two peaks are found, as expected, to be significantly more pronounced for NDI aromatic interactions in $W_{pH=7}$ and W/H solutions.

The CD spectra (Figure 2b) show the formation of stable β-sheet motifs for $\mathbf{P^{NDI}}$ self-assembly in all solutions, as deduced from the deep minima at 215–220 nm. Significant differences were, however, found in the Cotton effect peaks at 300–400 nm that correspond to the polarized transition along the NDI moiety *z* axis.[8f,15] For structures formed in W/A or $W_{pH=7}$ solutions, a positive Cotton effect was observed, associated with the *P* helical configuration of the NDI

  

moieties within the fibril core.[16] In contrast, for structures formed in W/H solution, a negative, almost opposite, Cotton effect was observed correlating with NDI groups *M* helicity. Interestingly, the spectrum obtained for $\mathbf{P^{NDI}}$ in pure water reflects an intermediate arrangement between, or recombination of, the above two structures.

Using atomic force microscopy (AFM, Figure 3) and scanning electron microscopy (SEM; Supporting Information, Figure S7) measurements, we found that $\mathbf{P^{NDI}}$ self-assembled into twisted fibril-like nanostructures when equilibrated in any one of the four solvent mixtures. However, these nanostructures differed, sometimes significantly, in their morphology, namely in their width and helix pitch length (Table 1), as well as in the helix twist direction (Figure 4). $\mathbf{P^{NDI}}$ self-assembly in W, $W_{pH=7}$, or W/A mixtures produced long (up to 7 μm) fibrils with typical widths of 3–6 nm (measured from the AFM *z* direction, Figure 3), correlating well with the formation of single bilayer fibril structures or bundling of two fibrils. In contrast, self-assembly in the W/H solution led to the formation of shorter (200–600 nm) and significantly thicker (ca. 25 nm) fibrils. The helix pitch length values measured from the same images again revealed the similarity between structures formed in the W and W/A mixtures ($P \approx 35$ nm). Less-twisted self-assembly products were found in the $W_{pH=7}$ and W/H solutions ($P = 50$ nm and 75 nm, respectively). AFM images at higher lateral resolution revealed the formation of both left and right helical twists (Figure 4; Supporting Information, Figure S8) for the fibril nanostructures formed in the different solutions. A statistical analysis performed on ≥100 fibers from each solution shows a clear preference for the formation of left helical fibers in $W_{pH=7}$ and W/A mixtures and right helical fibers in W/H solution, and almost no handedness preference for fibrils formed in distilled water (W). Remarkably, this trend correlates perfectly with the *P* versus *M* helicity trend observed in the CD measurements (Figure 2b).

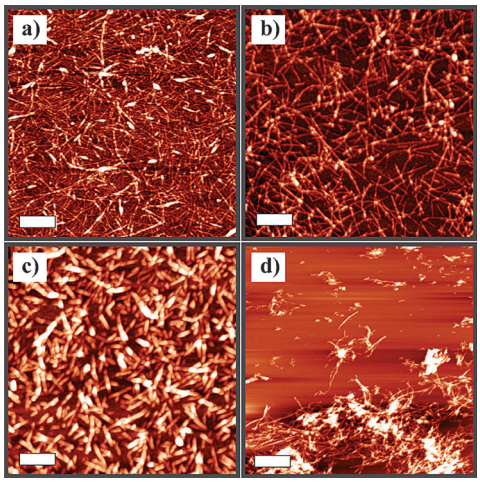


***Figure 3.*** AFM topography images of fibers formed after equilibration of $\mathbf{P^{NDI}}$ (350 μM) in W (a), W/A (b), W/H (c), and $W_{pH=7}$ (d) mixtures for 30 min. All scale bars are 500 nm.

***Table 1:*** Fibril characteristics for $\mathbf{P^{NDI}}$ assembled in the different mixtures.[a]

| Assembly conditions | W | W/A | W/H | $W_{pH=7}$ |
|---|---|---|---|---|
| Width [nm] | 3 ± 1 | 6 ± 1 | 24 ± 8 | 5 ± 1 |
| Pitch length [nm] | 37 ± 6 | 34 ± 7 | 74 ± 13 | 49 ± 10 |

[a] Data averaged from multiple fibril AFM images, as shown in Figure 3. For analysis methodology see SI.

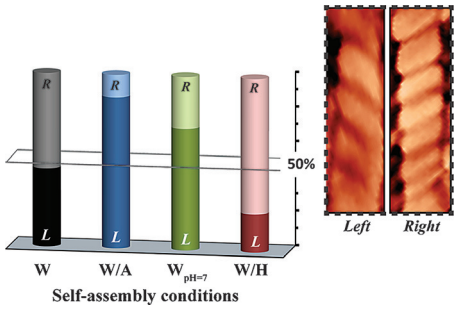


***Figure 4.*** Statistical handedness data analysis for fibrils formed in the various solvents (*L* and *R* helical twists fractions are represented by dark and light colors, respectively). Inset: examples of high-resolution AFM phase images presenting the left and right helical twists (additional images in the Supporting Information, Figure S8).

The densely packed core π-system of the fibrils suggests that they are uniquely suited to support electron transport. Electrical characterizations were performed using specifically designed chips with gold electrodes separated by gaps of $L =$ 5, 10, or 20 μm (Figure 5; Supporting Information, Figures S2 and S3). $\mathbf{P^{NDI}}$ self-assembled fibrils equilibrated in the various mixtures (W, W/A, and W/H), as well as control **KFE-8** fibrils formed in water, were drop-casted on the chips, forming dense networks bridging the gaps (Figure 5a).

Current–voltage (*I–V*) measurements revealed substantial currents for devices including $\mathbf{P^{NDI}}$ fibrils, while no currents were detected for **KFE-8** fibril devices within the measurement detection limit of about 0.1 pA (Figure 5b). This comparison indicates a conductivity enhancement of at least two orders of magnitude owing to the attachment of the NDI moiety. The current values that we obtained for the $\mathbf{P^{NDI}}$ assemblies were in the same range as those we previously reported for truncated β-amyloid peptides with non-natural thiophene[9e] or furan[17] modifications. Remarkably, we also detected significant differences in the conductivity of the $\mathbf{P^{NDI}}$ fibers formed in the different solvent mixtures (Figure 5b). The differences may be seen in the average ohmic conductance ($G = I/V$) of the networks formed under the W, W/A, and W/H conditions, respectively (Figure 5b, inset). The same trend was observed for the fibril networks deposited between the electrodes with the 10 and 20 μm gaps, albeit with lower currents with increasing gap sizes, as expected (Supporting Information, Figure S3). The length-dependent resistance of the system, extracted as $R_L = 1/G_L$ (Figure 5c), provides further insight into the fibril sheet resistance ($\rho/t$, where *t* is the effective network thickness), and the fibril–electrode contact resistance ($R_C$), as manifested in Equation (1), where *w* is the electrode width:[17]

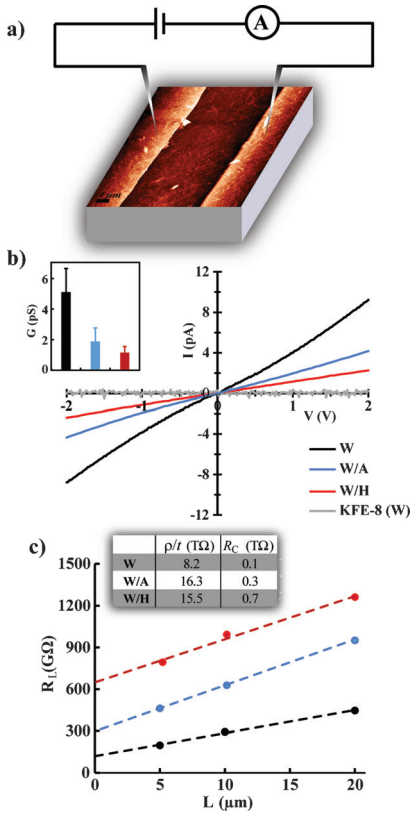


***Figure 5.*** Electronic characterization of $\mathbf{P^{NDI}}$. a) AFM image of a peptide fibril network covering the chip electrodes and the gap between them. The measurement setup is also represented schematically. b) Representative *I*–*V* curves of $\mathbf{P^{NDI}}$ fibrous networks formed after self-assembly in the various solvent mixtures, and control **KFE-8** network formed in pure water. Measurements were recorded under vacuum conditions with electrode gap of 5 μm. Inset: average conductance values (*G*) of the peptide networks deduced from the slope of the *I*–*V* curves. c) Resistance as a function of the gap length for $\mathbf{P^{NDI}}$ fibrous networks formed in the various mixtures. Inserted table shows the fibril–electrode contact resistance ($R_C$) and the bulk sheet resistance ($\rho/t$) extracted from this plot using Equation (1).

$$R_L = R_C + \frac{\rho L}{tw} \tag{1}$$

The results in Figure 5c show that both low contact resistance and sheet resistance afford the better conductivity observed for the assemblies formed in water (W). The assemblies formed under W/A and W/H conditions showed similar inherent bulk resistance properties but a more than twofold difference in the contact resistance, resulting in higher conductivity for the former system.

Taken together, our studies demonstrate that the self-assembly of peptide aromatics into fibrils is driven by a set of hydrogen-bonding and electrostatic and π-stacking interactions, governed by the solvent used for the assembly. The assembly process can be directed towards a distinct polymorph by using the medium to enhance specific type(s) of interactions over the others. Self-assembly in the W or W/A solutions is mostly governed by hydrogen bonding and electrostatic interactions, favoring β-sheet formation and leading to long fibrils, similar to those observed for **KFE-8** (Supporting Information, Figure S6). Indeed, assembly in acetonitrile–water mixtures has been previously shown to drive fast fibril growth while inhibiting the formation of bundled architectures.[12] In the polar W/H solution, HFIP creates a layer around the peptide molecules reducing the accessibility of the backbone hydrogen bonds to interact with other monomers.[8h,13] Hence, the assembly process is primarily driven by π-interactions. These, in turn, induce the formation of thicker fibrils, as well as alteration of the NDI moieties arrangement within the fibril core, even to the extent of complete chirality inversion.

The fibril conductivity is affected by the differences in both morphology and chirality. The formation of long thin fibrils in W and W/A networks accounts for their lower sheet and contact resistance, and thus better conductivity comparing to W/H. The effect of chirality-related polymorphism on conductivity may, hence, be determined by comparing the characteristics of W and W/A networks. The higher conductivity of W fibrils, despite similar length and width, is attributed to formation of racemic assemblies. This behavior implies that the right-handed fibrils promote conductivity. We note that this conductivity enhancement is possibly suppressed in W/H owing to the fibril morphology effects discussed above. Based on the findings of this study we suggest that the functionality of peptide fibril systems, such as electron conductivity and catalytic activity, can be fine-tuned by carefully controlling polymorphisms through the choice of the appropriate environmental assembly conditions.

## Acknowledgements

We thank Prof. D. T. Major and Dr. A. Vardi-Kilshtain (Bar-Ilan University) for computational support. We acknowledge BGU Kreitman School for Ph.D. fellowships (D.I., M.A.) and short term post doctorate fellowship (M.A.), and the COST action CM1304.

**Keywords:** bio-electronics · chemical evolution · peptide fibrils · polymorphism

**How to cite:** *Angew. Chem. Int. Ed.* **2016**, *55*, 9988–9992
*Angew. Chem.* **2016**, *128*, 10142–10146

[1] a) C. A. E. Hauser, S. G. Zhang, *Chem. Soc. Rev.* **2010**, *39*, 2780–2790; b) S. Cavalli, F. Albericio, A. Kros, *Chem. Soc. Rev.* **2010**, *39*, 241–263; c) J. B. Matson, S. I. Stupp, *Chem. Commun.* **2012**, *48*, 26–33; d) X. Du, J. Zhou, J. Shi, B. Xu, *Chem. Rev.* **2015**, *115*, 13165–13307.

[2] *Protein Misfolding Diseases: Current And Emerging Principles And Therapies* (Eds.: M. Ramirez-Alvarado, J. W. Kelly, C. M. Dobson), Wiley, **2010**.

[3] a) B. Rubinov, N. Wagner, H. Rapaport, G. Ashkenasy, *Angew. Chem. Int. Ed.* **2009**, *48*, 6683–6686; *Angew. Chem.* **2009**, *121*, 6811–6814; b) J. T. Goodwin, A. K. Mehta, D. G. Lynn, *Acc. Chem. Res.* **2012**, *45*, 2189–2199; c) G. Danger, R. Plasson, R. Pascal, *Chem. Soc. Rev.* **2012**, *41*, 5416–5429; d) J. W. Sadownik, E. Mattia, P. Nowak, S. Otto, *Nat. Chem.* **2016**, *8*, 264–269.

[4] a) S. Maude, E. Ingham, A. Aggeli, *Nanomedicine* **2013**, *8*, 823–847; b) M. C. Branco, D. M. Sigano, J. P. Schneider, *Curr. Opin. Chem. Biol.* **2011**, *15*, 427–434.

  

[5] J. Zhou, B. Xu, *Bioconjugate Chem.* **2015**, *26*, 987 – 999.
[6] a) B. Rubinov, N. Wagner, M. Matmor, O. Regev, N. Ashkenasy, G. Ashkenasy, *ACS Nano* **2012**, *6*, 7893 – 7901; b) C. M. Rufo, Y. S. Moroz, O. V. Moroz, J. Stoehr, T. A. Smith, X. Hu, W. F. DeGrado, I. V. Korendovych, *Nat. Chem.* **2014**, *6*, 303 – 309; c) C. Zhang, X. Xue, Q. Luo, Y. Li, K. Yang, X. Zhuang, Y. Jiang, J. Zhang, J. Liu, G. Zou, X.-J. Liang, *ACS Nano* **2014**, *8*, 11715 – 11723; d) N. Singh, M. Tena-Solsona, J. F. Miravet, B. Escuder, *Isr. J. Chem.* **2015**, *55*, 711 – 723; e) M. Tena-Solsona, J. Nanda, S. Diaz-Oltra, A. Chotera, G. Ashkenasy, B. Escuder, *Chem. Eur. J.* **2016**, *22*, 6687 – 6694.
[7] a) N. Ashkenasy, W. S. Horne, M. R. Ghadiri, *Small* **2006**, *2*, 99 – 102; b) J. D. Tovar, *Acc. Chem. Res.* **2013**, *46*, 1527 – 1537; c) H. A. M. Ardoña, J. D. Tovar, *Bioconjugate Chem.* **2015**, *26*, 2290 – 2302; d) A. Shah, B. Adhikari, S. Martic, A. Munir, S. Shahzad, K. Ahmad, H.-B. Kraatz, *Chem. Soc. Rev.* **2015**, *44*, 1015 – 1027.
[8] a) Y. Miller, B. Ma, R. Nussinov, *Chem. Rev.* **2010**, *110*, 4820 – 4838; b) J. S. Pedersen, C. B. Andersen, D. E. Otzen, *FEBS J.* **2010**, *277*, 4591 – 4601; c) D. Thirumalai, G. Reddy, J. E. Straub, *Acc. Chem. Res.* **2012**, *45*, 83 – 92; d) L. R. Volpatti, M. Vendruscolo, C. M. Dobson, T. P. J. Knowles, *ACS Nano* **2013**, *7*, 10443 – 10448; e) R. Tycko, R. B. Wickner, *Acc. Chem. Res.* **2013**, *46*, 1487 – 1496; f) S. Manchineella, V. Prathyusha, U. D. Priyakumar, T. Govindaraju, *Chem. Eur. J.* **2013**, *19*, 16615 – 16624; g) J. E. Smith, C. Liang, M. Tseng, N. Li, S. Li, A. K. Mowles, A. K. Mehta, D. G. Lynn, *Isr. J. Chem.* **2015**, *55*, 763 – 769; h) Y. Wang, W. Qi, R. Huang, X. Yang, M. Wang, R. Su, Z. He, *J. Am. Chem. Soc.* **2015**, *137*, 7869 – 7880.
[9] a) W. S. Horne, N. Ashkenasy, M. R. Ghadiri, *Chem. Eur. J.* **2005**, *11*, 1137 – 1144; b) S. R. Diegelmann, J. M. Gorham, J. D. Tovar, *J. Am. Chem. Soc.* **2008**, *130*, 13840 – 13841; c) H. Xu, A. K. Das, M. Horie, M. S. Shaik, A. M. Smith, Y. Luo, X. Lu, R. Collins, S. Y. Liem, A. Song, P. L. A. Popelier, M. L. Turner, P. Xiao, I. A. Kinloch, R. V. Ulijn, *Nanoscale* **2010**, *2*, 960 – 966; d) M. Mizrahi, A. Zakrassov, J. Lerner-Yardeni, N. Ashkenasy, *Nanoscale* **2012**, *4*, 518 – 524; e) M. Amit, G. Cheng, I. W. Hamley, N. Ashkenasy, *Soft Matter* **2012**, *8*, 8690 – 8696; f) J. A. Lehrman, H. Cui, W.-W. Tsai, T. J. Moyer, S. I. Stupp, *Chem. Commun.* **2012**, *48*, 9711 – 9713; g) Y. Tidhar, H. Weissman, S. G. Wolf, A. Gulino, B. Rybtchinski, *Chem. Eur. J.* **2011**, *17*, 6068 – 6075; h) S. Fleming, P. W. J. M. Frederix, I. Ramos Sasselli, N. T. Hunt, R. V. Ulijn, T. Tuttle, *Langmuir* **2013**, *29*, 9510 – 9515; i) Y. Zhang, B. Zhang, Y. Kuang, Y. Gao, J. Shi, X. X. Zhang, B. Xu, *J. Am. Chem. Soc.* **2013**, *135*, 5008 – 5011; j) S. K. M. Nalluri, C. Berdugo, N. Javid, P. W. J. M. Frederix, R. V. Ulijn, *Angew. Chem. Int. Ed.* **2014**, *53*, 5882 – 5887; *Angew. Chem.* **2014**, *126*, 5992 – 5997; k) D. Ivnitski, M. Amit, B. Rubinov, R. Cohen-Luria, N. Ashkenasy, G. Ashkenasy, *Chem. Commun.* **2014**, *50*, 6733 – 6736.
[10] a) J. S. Rudra, T. Sun, K. C. Bird, M. D. Daniels, J. Z. Gasiorowski, A. S. Chong, J. H. Collier, *ACS Nano* **2012**, *6*, 1557 – 1564; b) R. J. Swanekamp, J. T. M. DiMaio, C. J. Bowerman, B. L. Nilsson, *J. Am. Chem. Soc.* **2012**, *134*, 5556 – 5559.
[11] Y. Raz, B. Rubinov, M. Matmor, H. Rapaport, G. Ashkenasy, Y. Miller, *Chem. Commun.* **2013**, *49*, 6561 – 6563.
[12] C. L. Shen, R. M. Murphy, *Biophys. J.* **1995**, *69*, 640 – 651.
[13] D. Roccatano, M. Fioroni, M. Zacharias, G. Colombo, *Protein Sci.* **2005**, *14*, 2582 – 2589.
[14] a) M. R. Molla, S. Ghosh, *Chem. Eur. J.* **2012**, *18*, 1290 – 1294; b) H. Shao, M. Gao, S. H. Kim, C. P. Jaroniec, J. R. Parquette, *Chem. Eur. J.* **2011**, *17*, 12882 – 12885.
[15] T. C. Barros, S. Brochsztain, V. G. Toscano, P. Berci, M. J. Politi, *J. Photochem. Photobiol. A* **1997**, *111*, 97 – 104.
[16] N. Sakai, P. Talukdar, S. Matile, *Chirality* **2006**, *18*, 91 – 94.
[17] M. Amit, N. Ashkenasy, *Isr. J. Chem.* **2014**, *54*, 703 – 707.

Received: May 17, 2016
Published online: July 8, 2016

  